Planned Nanostructures of Colloidal Gold via Self-Assembly on Hierarchically Assembled Organic Bilayer Template Patterns with In-situ Generated Terminal Amino Functionality

Shantang Liu, Rivka Maoz, and Jacob Sagiv*

Department of Materials and Interfaces, The Weizmann Institute of Science, Rehovot 76100, Israel

Received February 12, 2004

ABSTRACT

We demonstrate a hierarchical self-assembly approach to the fabrication of planned nanostructures of colloidal gold particles on silicon, comprising the initial assembly of a molecular template pattern with terminal amino functionality, which then guides the surface assembly and site specific anchoring of gold nanoparticles from a colloidal solution. Well defined amino-terminated templates are obtained via a chemical functionalization process whereby highly ordered bilayer nanopatterns produced by *constructive nanolithography* (Maoz, R.; Frydman, E.; Cohen, S. R.; Sagiv, J. *Adv. Mater.* 2000, *12*, 725–731) are in-situ modified to generate the top amine functions. This novel approach offers promising performance in terms of the precision, reproducibility, and structural robustness needed for the advancement of a reliable bottom-up nanofabrication methodology.

The planned assembly of surface-immobilized architectures of metal nanoparticles and their effective electrical connection to addressable contact electrodes constitutes a main challenge en route to the "bottom-up" fabrication of nano-metallic components for future nanodevices.[1,2] Research efforts have thus been invested in devising methods for the deliberate organization and immobilization of metal nanoparticles on solid surfaces. For example, it was shown that gold nanoparticles bearing various organic ligands can be anchored to solid surfaces functionalized with organic layers exposing appropriate binding functions.[1,3−5] Using patterned organic layer coatings produced by a number of different techniques, on different target surfaces, it was further possible to demonstrate the assembly of some planned surface arrangements of such nanoparticles.[6,7] However, despite the progress achieved in demonstrating these possibilities, the organic linker systems so far utilized for this purpose cannot provide the fine precision and high reproducibility needed for the reliable fabrication of planned two- and three-dimensional (2D, 3D) assemblies of metal nanoparticles that could become useful nanodevice components. Advancing a quantitative approach to the planned self-assembly of well-defined molecular templates, the structure and properties of

which can be tailored and reproduced with molecular precision, is therefore a prerequisite for their successful utilization. This remains a challenging task to be yet achieved. Another key issue that awaits to be addressed within the context of device fabrication has to do with the proper electrical insulation of the various nanometallic functional assemblies positioned on a solid substrate, which may limit the possible use of systems assembled on highly conductive substrate materials such as gold.[7]

In a series of exploratory studies reported from this laboratory, the potential of a generic methodology referred to as *constructive nanolithography* has been demonstrated,[8−11] whereby quantitative techniques of hierarchical mono-to-multilayer self-assembly and surface chemical modification[12,13] are combined with a novel monolayer patterning technique that allows chemical information to be inscribed on the outer surface of an organic self-assembled monolayer on silicon.[14] Constructive nanolithography exploits the observation that top-functionalized monolayer nanopatterns of any predefined geometrical design can be generated via nondestructive local electrochemical surface transformations carried out with the assistance of a conductive SFM (scanning force microscope) tip.[9,14,15] Tip-mediated local oxidation of the top −CH$_3$ groups of a highly ordered monolayer of OTS (*n*-octadecyltrichlorosilane) self-assembled on silicon was

* Corresponding author. E-mail: jacob.sagiv@weizmann.ac.il. Phone: +972-8-9342309. Fax: +972-8-9344138.
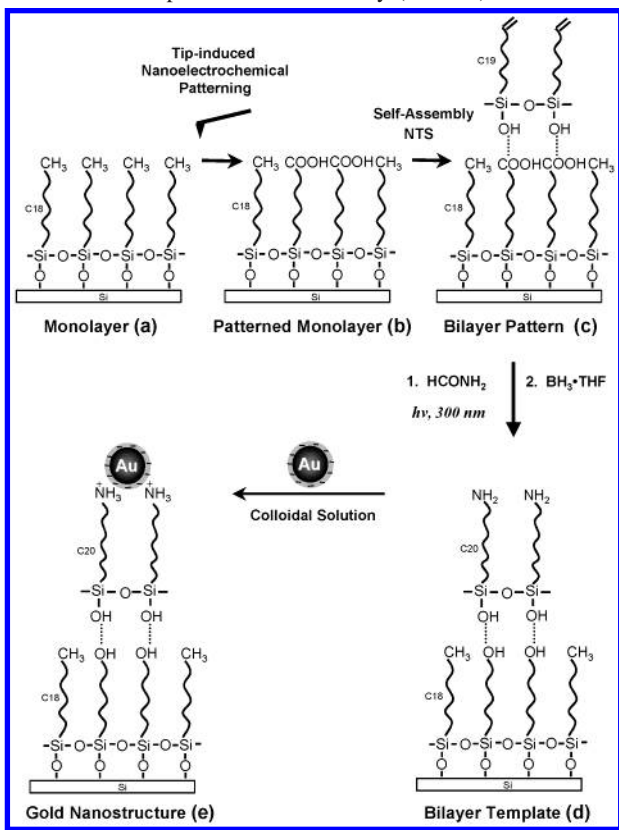
This schematic sketch (not drawn to scale) emphasizes some of the salient features of the investigated system that bear direct relevance to the present nanofabrication strategy; it does not represent a real chemical-structural model, particularly as far as the exact molecular arrangement and intermolecular bonding are concerned.[13,20]

thus used to inscribe nanopatterns of active −COOH functions on an inert background of unmodified −CH₃ groups.[9] Such tip-inscribed −COOH patterns have high chemical, thermal, and mechanical stability, which makes possible their use as templates in further template-assisted assembly steps.[9,10,16] However, the mere use of the −COOH terminal functionality generated in the initial patterning process restricts the choice of useful post-patterning routes for template-assisted assembly of diverse inorganic nanoentities. Other functional groups of interest were therefore installed via further chemical derivatization and development of the initial tip-inscribed sites.[9] Thus, the in-situ chemical functionalization of an ordered vinyl-terminated overlayer (NTS, nonadecenyltrichlorosilane) self-assembled on the −COOH sites inscribed on a base OTS monolayer was previously used to generate elevated −S−S− (disulfide) and −SH (thiol) copies of the initial pattern.[9–11] These sulfur-functionalized patterns form templates capable of guiding the subsequent surface self-assembly of inorganic species such as nanoparticulate CdS,[9,10] silver[9] and gold,[10,11] in-situ generated on the template,[9,10,17] or ex-situ synthesized.[11] We
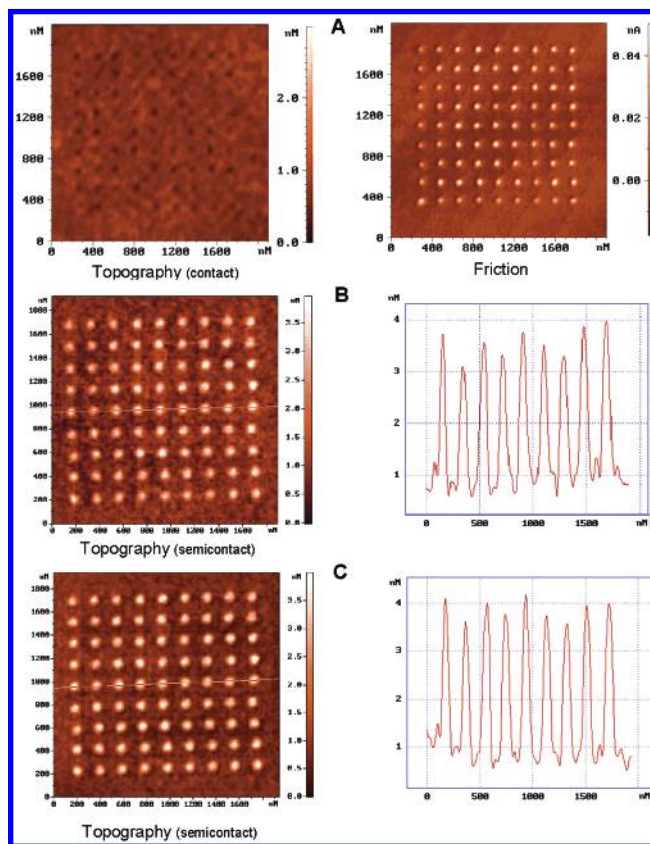
Figure 1. Monolayer and bilayer patterns produced by the stepwise assembly process depicted in Scheme 1. (A) Topographic and simultaneously acquired friction (lateral force) contact-mode SFM images (left and right side, respectively) of an array of 9×9 dots, corresponding to step (b) in Scheme 1. The pattern inscription was done with 400×400 raster-scanned points/patterned area, by applying 3.0 ms/point voltage pulses, at a positive surface bias of 8.8 V relative to the tip (W₂C-coated conductive probes with normal spring constants of 0.15−1.5 N/m, operated in the contact mode in a controlled humidity atmosphere of ∼60% relative humidity).[21] (B) Semicontact mode SFM topographic image of the dot array shown in A and distance-height profiles along the marked line, taken after the assembly of the bilayer pattern (step (c) in Scheme 1).[21] (C) Image of the bilayer pattern and the corresponding distance−height profiles as shown in B, after the generation of the top amino functionality (step (d) in Scheme 1).[19] A SOLVER P47 instrument (NT-MDT, Moscow, Russia) was used for both patterning and imaging. The contact mode images were acquired immediately after the inscription of the pattern, with the same W₂C-coated probe (without electrical bias and minimal contact force), and the semicontact mode ones with regular silicon probes (Silicon-MDT), in the ambient atmosphere. Lateral dimensions were estimated from the half-height widths measured across the distance−height or distance−friction (not shown) profiles of the various features of interest.

envision a number of different useful routes for the template-guided assembly of gold nanoparticles, each of which offering specific advantages for different specific applications. For example, ex-situ synthesized [Au₅₅] clusters representing well defined gold "supramolecules" with a metal core made of only 55 atoms (∼1.4 nm diameter) were successfully organized by guided self-assembly on such thiol-terminated bilayer template patterns, the specific adherence of [Au₅₅] to the thiolated surface sites relying on a mechanism of ligand exchange.[11]
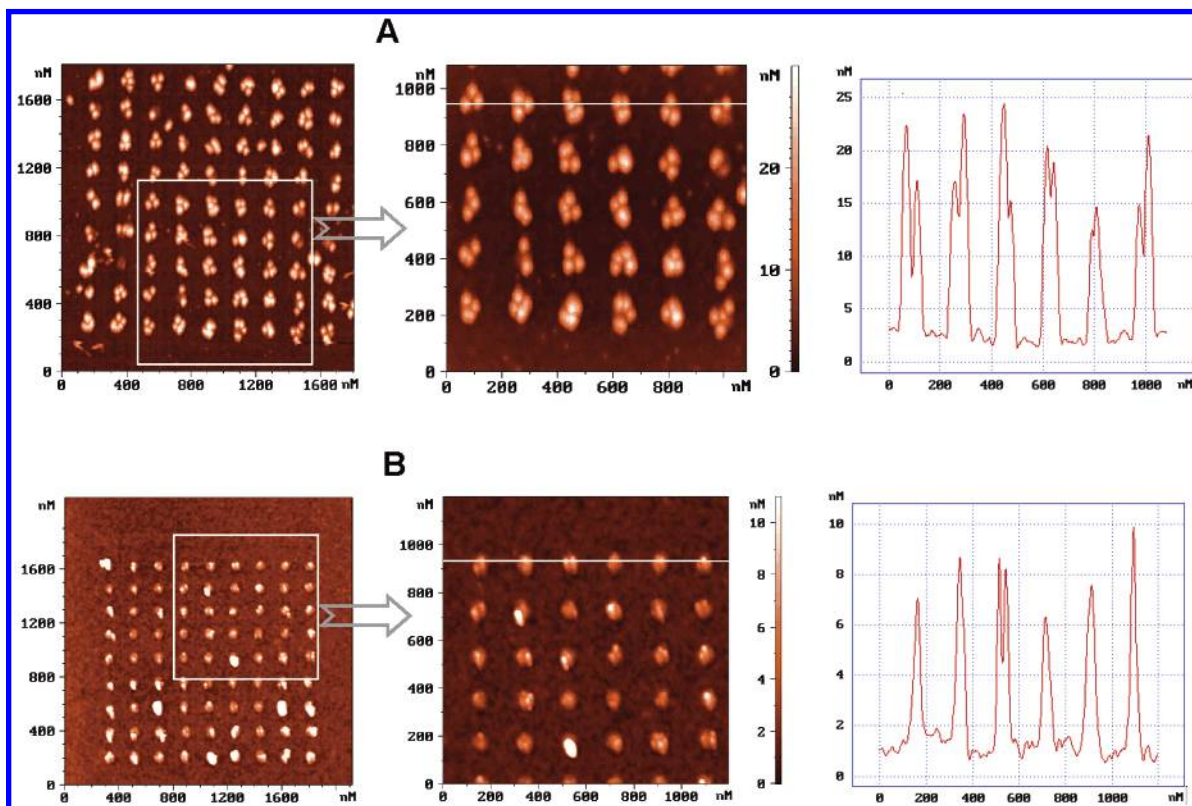
Figure 2. Semicontact mode SFM topographic images (acquired as in Figure 1) of gold nanostructures representing colloidal gold particles self-assembled on amino-terminated bilayer template patterns (step (e) in Scheme 1). (A) Left side, ~17 nm [Au-citrate] particles[22] self-assembled on the dot array shown in Figure 1C (6 h immersion in the colloidal gold solution). Middle, detailed scan of the marked square area in the left side image. Right side, distance–height profiles along the marked line in the middle image. (B) As in A, showing 2–6 nm [Au-citrate] particles[23] self-assembled on a similarly prepared array of 81 dots (10 min immersion in the colloidal gold solution). Lateral dimensions were estimated from the corresponding distance–height profiles, as indicated in Figure 1.

Here we examine a different process for the site-defined surface self-assembly of prefabricated gold nanoparticles, via electrostatic attraction between negatively charged colloidal [Au-citrate] particles and positively charged bilayer template patterns with top $-NH_2$ functions[3,4] (Scheme 1). To generate well-defined amino-terminated template patterns, the structure and properties of which can be reproduced and controlled with molecular precision, we adopted an approach analogous to that previously used for the generation of sulfur-terminated templates,[9–11] consisting of the in-situ chemical functionalization of a high quality precursor overlayer assembled on the tip-inscribed monolayer pattern of interest. This was accomplished by photoreacting the terminal vinyl groups of a precursor NTS overlayer with formamide, which adds a terminal amide group to the hydrocarbon tail of NTS,[18] and its further reduction with $BH_3·THF$ to the terminal amino functionality. Based on previous results obtained in this laboratory,[19] it was expected that this synthetic route (c → d in Scheme 1) should preserve the high molecular order of the precursor NTS overlayer while effecting the conversion of NTS to the corresponding amino-terminated C20 silane[19] and the reduction of the interlayer $-COOH$ groups (generated in the initial pattern inscription process) to $-CH_2OH$.[19,20]

The overall fabrication process depicted in Scheme 1 explores the organization of water-soluble [Au-citrate] colloidal particles on amino-terminated template patterns produced by the present in-situ chemical functionalization of

preassembled NTS bilayer patterns.[19,21] [Au-citrate] colloidal particles were synthesized by the reduction of $AuCl_4^-$ with trisodium citrate, according to the procedures described by Frens[22] and Natan.[23] By varying the conditions of the synthesis, it was possible to obtain different size distributions of such particles. The template-guided assembly of the gold particles was carried out by immersing the silicon wafer specimens bearing the template patterns into the colloidal solutions (for periods of time of 10 min or 6 h), followed by ~5 min rinse in a flow of pure water. Colloidal gold particles synthesized by this process acquire negative charge due to the adsorption of citrate and chloride anions present in the colloidal suspension, while protonation of the surface amino groups results in positive charging of the template.[3] Therefore, the spontaneous assembly of the [Au-citrate] particles on the amino-terminated template patterns appears to be driven by the electrostatic attraction between oppositely charged template and metal particles. It may thus be expected that post-assembly removal or exchange of the thin citrate ligand shell would eventually allow the formation of densely packed arrangements of gold nanoparticles on the template sites.[3]

SFM images demonstrating the successful fabrication of amino-terminated bilayer templates and the subsequent template-guided assembly of nanoparticulate gold structures with different predefined geometrical shapes (dots, wires, pads) are given in Figures 1–4. Figure 1 shows images of
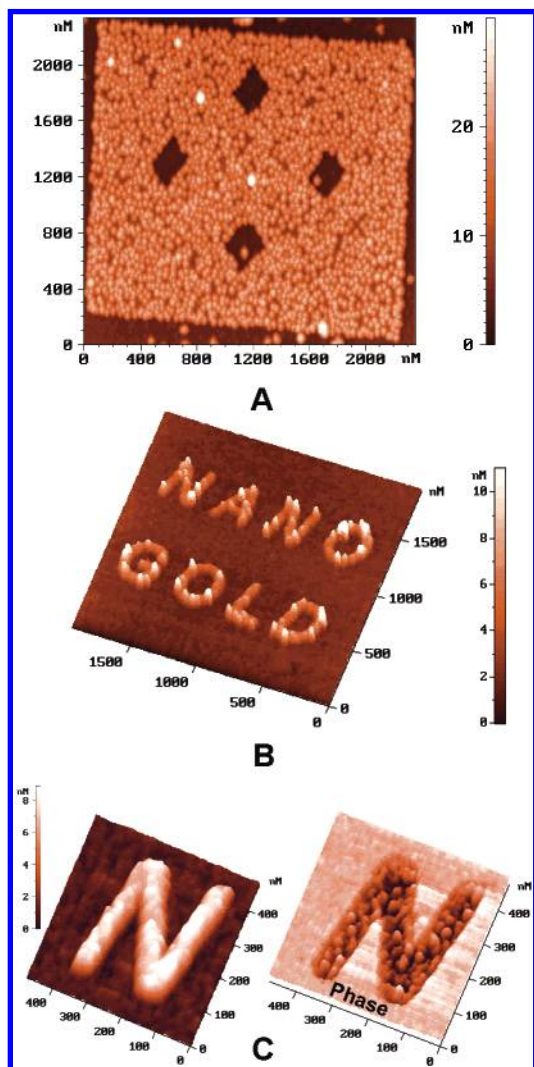
Figure 3. Semicontact mode topographic images of colloidal gold nanostructures (fabricated and imaged as those shown in Figure 2). (A) ~17 nm [Au-citrate] particles self-assembled on a bilayer pad pattern with four unmodified OTS rhombuses (same specimen as in Figure 2A). (B) 2−6 nm [Au-citrate] particles self-assembled on a bilayer letter pattern (same specimen as in Figure 2B). The pattern inscription conditions were as in Figure 1, with applied tip−surface biases of 6.5 V in A and 7.5 V in B. (C) Detailed scan showing both topographic (left side) and phase images of the first "N" in a letter pattern of small particles such as that in B above (produced with 6 h immersion in the colloidal gold solution), after Scotch-tape treatment.

an array of 9×9 dots, corresponding to steps (b), (c), and (d) of Scheme 1. As expected,[9] the array pattern inscribed on the OTS base monolayer displays high friction contrast in the lateral force image (with an apparent lateral dot size of ca. 40 ± 4 nm) while being weakly visible in the corresponding topographic image (Figure 1A). Although the nondestructive tip-induced oxidation of the top monolayer surface does not affect significantly the surface topography (Scheme 1b), the dots are weakly visible also in the topographic image, albeit with a small negative contrast of 2−3 Å below the background of the unmodified monolayer. This is an artifact of the SFM imaging process, caused by friction-topography "crosstalk" and spot-to-spot force variations arising from the different hydration and adhesion properties of the polar (modified) and nonpolar (unmodified) regions in such heterogeneous surfaces.[24] The selective self-assembly of NTS on the oxidized surface sites of the OTS base monolayer (b → c in Scheme 1), gives rise to an elevated overlayer copy of the initial dot pattern inscribed by the tip (Figure 1B). It is expected that patterns in which the oxidation of the top −CH$_3$ groups of OTS to −COOH is complete correlate with the formation of a complete, well ordered overlayer of densely packed and perpendicularly oriented NTS molecules, with a height of ~2.7 nm,[25] whereas a partial reaction would result in an incomplete and less ordered top layer, with significantly lower height.[26] The SFM-measured heights of each of the 81 dots, before and after the conversion of the NTS overlayer to the amino-terminated template (Figure 1B and 1C, respectively), are 2.7 ± 0.3 nm and 3.0 ± 0.3 nm, respectively. These average and standard deviation values are in good agreement with the layer thickness and roughness parameters determined from X-ray scattering data of well-ordered monolayer films of NTS[25] and other long tail organosilanes with top polar functions derived from NTS,[13,19,20] the ~3 Å height increase upon the amination of NTS (compare the height profiles in Figure 1B and 1C) being a reasonable value, expected from the addition of one carbon atom and the amino group (Scheme 1).[19] Several of the extreme observed dot heights fall, however, within the range 2.1−3.4 nm and respectively 2.4−3.8 nm, for the unreacted and the amino-terminated overlayer. Taking into account the typical observed roughness of the base OTS/Si monolayers in the present SFM images (peak-to-peak features within ca. 0.5 nm),[27] these larger variations may reflect possible variations in the patterning, overlayer assembly, and amination processes, the precise control of which needs still to be improved. This analysis allows us to conclude that the synthetic route depicted in Scheme 1 is indeed compatible with the planned assembly of high quality bilayer features that preserve their structural integrity and molecular organization upon the quantitative in-situ generation of the top amino functionality. It further suggests that the apparent lateral broadening of the dots from ca. 40 ± 4 nm in Figure 1A to ca. 64 ± 11 nm in Figure 1B and 1C (as estimated from the half-height widths of the corresponding friction and topographic cross-section profiles) has to do with the common SFM artifact caused by the convolution with the tip, rather than with an inexplicable real broadening of the initially inscribed features.

Some representative examples of planned patterns of colloidal gold particles (17 ± 2 nm and 2−6 nm) fabricated by the present method are given in Figures 2−4. These include different sizes and geometrical shapes, which serve to illustrate the organization of the [Au-citrate] on the amino template. The anchoring of the gold nanoparticles to the surface is seen to faithfully follow the initial tip-inscribed patterns, thus confirming the validity of the template-guided self-assembly strategy depicted in Scheme 1. A comparative analysis of the SFM images of the different fabricated patterns reveals the deposition of a single layer of gold nanoparticles on the amino template patterns. The individual particles distinguishable in Figures 2A and 3A are rather
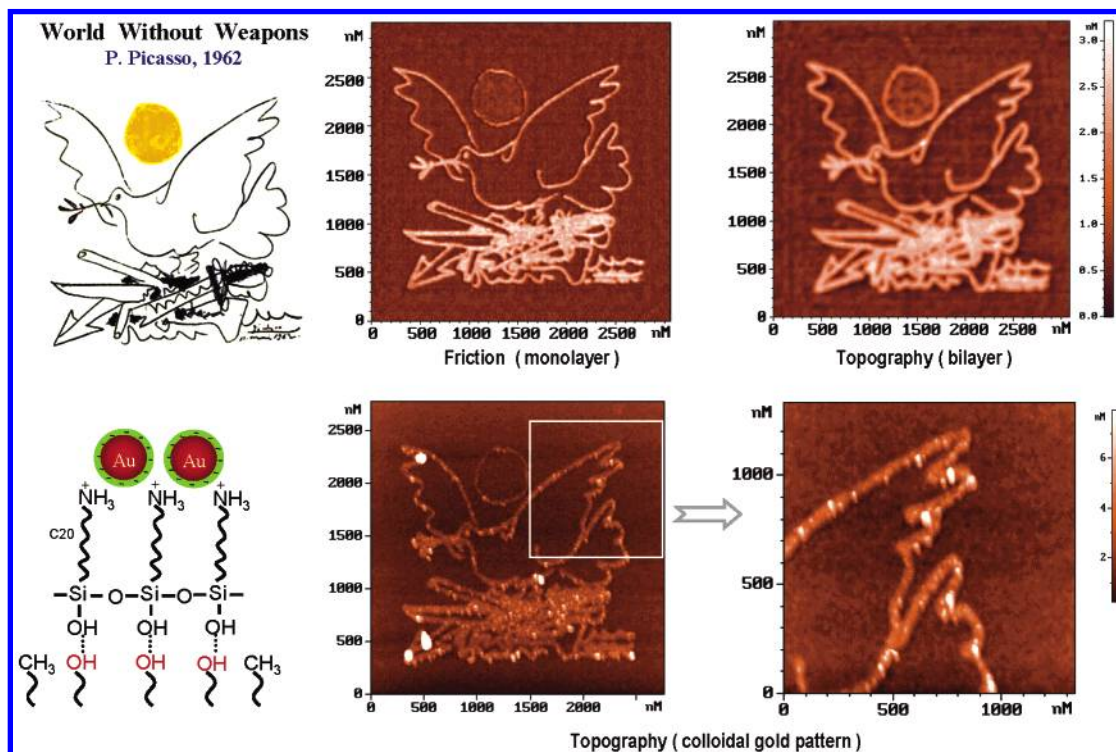
Figure 4. Example of more complex metal−organic nanoarchitecture fabricated via the template-guided hierarchical self-assembly route depicted in Scheme 1. Created by Picasso in 1962, the poster entitled "World Without Weapons" was downloaded from an Internet site (upper-left) and then translated into an input signal to the conducting SFM tip that inscribes (contact mode, line width ∼30 nm) a corresponding pattern of −COOH groups on the top surface of an OTS/Si monolayer specimen (step (b) in Scheme 1) − the Friction (monolayer) image. Topography (bilayer): semicontact mode image of the bilayer pattern resulting from the self-assembly of an NTS overlayer on the patterned monolayer (step (c) in Scheme 1). Topography (colloidal gold pattern): semicontact mode images of the final metal-organic composite nanostructure resulting from the self-assembly of 2−6 nm [Au-citrate] particles (same specimen as in Figure 2B) on the amino-terminated bilayer template (lower left sketch, corresponding to step (e) in Scheme 1). Individual gold particles specifically deposited on the dove wing and tail are clearly seen in the lower-right image, showing a detailed scan of the marked square area in the full-size image (middle). The pattern inscription and imaging were carried out as described in Figure 1, with 800×800 raster-scanned points (3.3 ms/point), at a tip−surface bias of 8.5 V.

uniform, with measured heights of ∼17 ± 2 nm and apparent lateral dimensions of ∼32 ± 3 nm. Since these colloidal particles have approximately spherical shapes[3,4] and there is good agreement between their SFM-measured heights and the average metal core diameter derived from X-ray scattering data of such particles assembled on unpatterned amino-terminated monolayer surfaces prepared by the present method (15.5−16.1 nm),[19] we may safely conclude that, as observed before,[4] the SFM-measured lateral dimensions are exaggerated by the convolution with the imaging tip. This conclusion is further corroborated by the observation that each template dot in Figure 2A accommodates between two to four apparently touching particles, their added lateral size (∼70 nm) correlating well with the apparent lateral size of the respective dot templates (∼64 nm, Figure 1C). However, estimating the real lateral size of the dots on the basis of the actual diameters of the template-anchored gold particles (∼17 nm) gives values closer to 40 nm, i.e., similar to the size of the initial tip-inscribed dot features (Figure 1A). The good agreement between the lateral dimensions of the tip-inscribed features estimated from either the half-height widths of the corresponding friction cross-section profiles (not shown) or the added diameters of the anchored metal particles (i.e., their SFM-measured heights) may thus be taken as a further

indicator of the validity of the estimates based on these considerations.

The small particles assembled on dots (Figure 2B) and on the more complex line patterns (Figures 3B, 3C and 4) are seen to have less uniform size, occasionally forming also coalesced aggregates. With individual particles sizes in the range 2−6 nm (as estimated from their SFM-measured heights) and apparent lateral dimensions of the order of ∼25 nm, the resolution of closely located such particles becomes difficult. While the presence of more than one particle per dot is generally apparent in the 9×9 dot array in Figure 2B, a reliable determination of the average number of particles assembled on each dot is thus not possible.

The [Au-citrate] assembly on the amino bilayer template patterns, apparently driven by electrostatic interactions only, results in gold/template structures displaying rather high stability under exposure to different organic solvents, acids, and bases, such as 5% aqueous HCl or HNO$_3$, 5% NaOH or KOH, the RCA silicon cleaning method, and sonication. Particles below a certain size also show high stability with respect to Scotch-tape peeling, contrary to larger particles that may be removed by such treatment from the surface. For example, a comparative inspection of Figure 3B and 3C clearly indicates that nanoparticles left on the surface of a

Scotch-tape treated sample (Figure 3C) are smaller and their size distribution more uniform, with measured heights of ~2.2 ± 0.5 nm and apparent lateral dimensions (estimated from the phase image) of ~15 ± 5 nm.

In conclusion, the template-guided self-assembly of colloidal gold nanoparticles on bilayer template patterns produced by the present hierarchical assembly approach offers significantly improved performance in terms of the structural precision, the reproducibility and the overall stability needed for the reliable chemical fabrication of functional components for future nanodevice applications. The results obtained suggest that further improvements in the control of the lateral dimensions of tip-inscribed features should make possible the reproducible positioning of single gold nanoparticles on preselected template dots, as well as the assembly of single rows of such particles on template line patterns designed for this purpose. To achieve this, the lateral size of the selected dot or line template should not exceed the size of the particles to be immobilized, which, for spherical particles, can be reliably estimated from their SFM-determined heights. Future efforts in this direction will have to focus on the use of sharper tips and the exploration of patterning conditions that may lead to a reduction in the lateral size of the inscribed features. A conceptually more advanced "self-patterning" approach, based on templates with active/inert mixed functionality, would allow achieving lateral dilution and spontaneous phase-separation of the binding functions within laterally confined surface domains, thus enabling fine-tuning of pattern formation below the lowest limits characteristic of the tip-induced patterning process itself.[28] We should finally emphasize that the use of well defined molecular templates, the vertical extensions of which can be adjusted with subnanometer precision, offers rather unique capabilities for fine-tuning of distances between surface anchored nanoobjects such as colloidal metal particles, via their precise vertical positioning above the substrate surface. This attractive feature of the present approach, demonstrated here for the simple case of a single molecular overlayer with a characteristic height of the order of 3 nm, suggests interesting possibilities for the advancement of a 3D chemical nanofabrication methodology based on the hierarchical self-assembly of planned multilayer molecular templates.[29]

References

(1) *Nanoparticles and Nanostructured Films*; Fendler, J. H., Ed.; Wiley-VCH: Weinheim, 1998. Schmid, G.; Chi, L. F. *Adv. Mater.* **1998**, *10*, 515−526. Shipway, A. N.; Katz, E.; Willner, I. *ChemPhysChem* **2000**, *1*, 18−52. Fendler, J. H. *Chem. Mater.* **2001**, *13*, 3196−3210.

(2) Simon, U. *Adv. Mater.* **1998**, *10*, 1487−1492. Schmid, G.; Liu, Y.-P.; Schumann, M.; Raschke, T.; Radehaus, C. *Nano Lett.* **2001**, *1*, 405−407.

(3) Doron, A.; Katz, E.; Willner, I. *Langmuir* **1995**, *11*, 1313−1317. Freeman, R. G.; Grabar, K. C.; Allison, K. J.; Bright, R. M.; Davis, J. A.; Guthrie, A. P.; Hommer, M. B.; Jackson, M. A.; Smith, P. C.; Walter, D. G.; Natan, M. J. *Science* **1995**, *267*, 1629−1632. Sato, T.; Brown, D.; Johnson, B. F. G. *Chem. Commun.* **1997**, 1007−1008. Zhu, T.; Fu, X.; Mu, T.; Wang, J.; Liu, Z. *Langmuir* **1999**, *15*, 5197−5199. Yonezawa, T.; Onoue, S.; Kunitake, T. *Adv. Mater.* **1998**, *10*, 414−416. Liu, S.; Zhu, T.; Hu, R.; Liu, Z. *Phys. Chem. Chem. Phys.* **2002**, *4*, 6059−6062.

(4) Grabar, K. C.; Allison, K. J.; Baker, B. E.; Bright, R. M.; Brown, K. R.; Freeman, R. G.; Fox, A. P.; Keating, C. D.; Musick, M. D.; Natan, M. J. *Langmuir* **1996**, *12*, 2353−2361. Grabar, K. C.; Brown, K. R.; Keating, C. D.; Stranick, S. J.; Tang, S.-L.; Natan, M. J. *Anal. Chem.* **1997**, *69*, 471−477.

(5) Fan, H.; López, G. P. *Langmuir* **1997**, *13*, 119−121. Taton, T. A.; Mucic, R. C.; Mirkin, C. A.; Letsinger, R. L. *J. Am. Chem. Soc.* **2000**, *122*, 6305−6306.

(6) Vossmeyer, T.; DeIonno, E.; Heath, J. R. *Angew. Chem., Int. Ed. Engl.* **1997**, *36*, 1080−1083. Zheng, J.; Zhu, Z.; Chen, H.; Liu, Z. *Langmuir* **2000**, *16*, 4409−4412. Hoeppener, S.; Chi, L.; Fuchs, H. *Nano Lett.* **2002**, *2*, 459−463. Lu, N.; Gleiche, M.; Zheng, J.; Lenhert, S.; Xu, B.; Chi, L.; Fuchs, H. *Adv. Mater.* **2002**, *14*, 1812−1815. Li, Q.; Zheng, J.; Liu, Z. *Langmuir* **2003**, *19*, 166−171.

(7) He, H. X.; Zhang, H.; Li, Q. G.; Zhu, T.; Li, S. F. Y.; Liu, Z. F. *Langmuir* **2000**, *16*, 3846−3851. Demers, L. M.; Park, S.-J.; Taton, T. A.; Li, Z.; Mirkin, C. A. *Angew. Chem., Int. Ed.* **2001**, *40*, 3071−3073. Garno, J. C.; Yang, Y.; Amro, N. A.; Cruchon-Dupeyrat, S.; Chen, S.; Liu, G.-Y. *Nano Lett.* **2003**, *3*, 389−395.

(8) Maoz, R.; Frydman, E.; Cohen, S. R.; Sagiv, J. *Adv. Mater.* **2000**, *12*, 424−429.

(9) Maoz, R.; Frydman, E.; Cohen, S. R.; Sagiv, J. *Adv. Mater.* **2000**, *12*, 725−731.

(10) Hoeppener, S.; Maoz, R.; Cohen, S. R.; Chi, L.; Fuchs, H.; Sagiv, J. *Adv. Mater.* **2002**, *14*, 1036−1041.

(11) Liu, S.; Maoz, R.; Schmid, G.; Sagiv, J. *Nano Lett.* **2002**, *2*, 1055−1060.

(12) Sagiv, J. *J. Am. Chem. Soc.* **1980**, *102*, 92−98. Netzer, L.; Sagiv, J. *J. Am. Chem. Soc.* **1983**, *105*, 674−676. Maoz, R.; Sagiv, J. *J. Colloid Interface Sci.* **1984**, *100*, 465−496. Maoz, R.; Netzer, L.; Gun, J.; Sagiv, J. *J. Chim. Phys.* **1988**, *85*, 1059−1065. Maoz, R.; Yam, R.; Berkovic, G.; Sagiv, J. In *Thin Films,* Vol. 20; Ulman, A., Ed.; Academic Press: San Diego, 1995; pp 41−68.

(13) Maoz, R.; Sagiv, J.; Degenhardt, D.; Möhwald, H.; Quint, P. *Supramol. Sci.* **1995**, *2*, 9−24. Baptiste, A.; Gibaud, A.; Bardeau, J. F.; Wen, K.; Maoz, R.; Sagiv, J.; Ocko, B. M. *Langmuir,* **2002**, *18*, 3916−3922.

(14) Maoz, R.; Cohen, S. R.; Sagiv, J. *Adv. Mater.* **1999**, *11*, 55−61.

(15) Pignataro, B.; Licciardello, A.; Cataldo, S.; Marletta, G. *Mater. Sci. Eng., C* **2003**, *23*, 7−12.

(16) Wouters, D.; Schubert, U. S. *Langmuir* **2003**, *19*, 9033−9038.

(17) Maoz, R.; Liu, S.; Sagiv, J., to be submitted for publication.

(18) Elad, D.; Rokach, J. *J. Org. Chem.* **1964**, *29*, 1855−1859.

(19) Unpatterned NTS monolayers on large silicon and fused silica surfaces were first used to investigate the quantitative in-situ conversion of NTS into a corresponding amino-terminated C20 silane that preserves the molecular organization of its vinyl-terminated precursor (Maoz, R.; Liu, S.; Sagiv, J., to be submitted for publication), as well as the subsequent self-assembly of [Au-citrate] particles on amino-terminated monolayer templates obtained in this manner (Baptiste, A., Ph.D. Thesis, Université du Maine, France, June, 2003. Baptiste, A.; Maoz, R.; Liu, S.; Gibaud, A.; Sagiv, J., to be submitted for publication). In these studies it was thus possible to apply, besides SFM, a series of powerful macroscopic methods of chemical and structural surface analysis, such as FTIR and UV−vis spectroscopies, XPS, X-ray reflectivity, and grazing incidence small-angle X-ray scattering (GISAXS).

(20) Previous studies carried out in this laboratory have demonstrated the possible in-situ reduction of the interlayer −COOH functions of an entire preassembled organosilane multilayer to −CH₂OH, and their back oxidation to −COOH, with good preservation of the overall molecular organization of the multilayer (Maoz, R.; Sagiv, J., unpublished results. Wen, K., Ph.D. Thesis, Weizmann Institute, Israel, April 1999. Wen, K.; Maoz, R.; Cohen, H.; Sagiv, J.; Gibaud, A.; Desert, A.; Ocko, B. M., to be submitted for publication).

(21) We found that prolonged exposures of OTS/Si base monolayers to high humidity conditions, as may frequently happen during repeated inscriptions of patterns on a particular specimen held in a controlled humidity atmosphere, induce their partial lateral reorganization into somewhat denser and better ordered molecular structures, which leaves a corresponding small uncovered fraction (~3%) of the total surface area. The monolayer-uncovered sites are tiny pinhole defects that cannot be detected by regular SFM imaging, however, if filled

up with NTS, their presence is revealed following the amination step and the exposure to the colloidal [Au-citrate] solution, as a result of their decoration by adsorbed gold particles. Thus, gold particles would detrimentally adhere to such defect sites dispersed within unpatterned regions of the OTS base monolayer. Improved OTS base monolayers, free of this undesirable effect, could be assembled by filling the pinhole defects with OTS, followed by adequate stabilization of the densified OTS structure obtained in this manner. Details of the assembly of such improved base monolayers will be given in a forthcoming publication (Maoz, R.; Liu, S.; Sagiv, J.). Briefly, the procedure applied in the present work consists of the following steps: (i) OTS monolayers were assembled on double-side-polished p-type silicon wafer substrates (Semiconductor Processing Co., 0.5 mm thick, orientation <100>, resistivity 8−11 Ωcm), by twice immersing the freshly cleaned hydrophilic substrate for ca. 30 s in a solution of OTS (5 mM) in pure bicyclohexyl (BCH), followed by sonication for ca. 2 min in analytical-grade toluene; (ii) densification and stabilization, by exposure of the OTS-coated specimen for 12 h to a 100% relative-humidity atmosphere (40 °C), followed by additional immersion in the OTS solution for ca. 30 s, sonication in toluene, and final annealing for 10 min in a preheated oven at 115 °C. This sequence of operations is repeated three times, ending with the thermal annealing at 115 °C. Such densified OTS/Si monolayers contain ∼3% more material than those produced without densification (as determined by quantitative infrared measurements) and display hysteresis-free static contact angles (equal advancing and receding values) of 116°−117° for water, 57° for bicyclohexyl, and 53° for *n*-hexadecane. These contact angle values are slightly but consistently higher (by 1°−2°) than those measured on same OTS/Si monolayers prior to their densification and stabilization. The assembly of NTS on the tip-inscribed monolayer patterns was done using the same procedure as in the assembly of the base OTS monolayer (without the densification/stabilization steps), by complete immersion of the patterned specimen in the NTS solution and final sonication in toluene.

(22) Frens, G. *Nature Phys. Sci*. **1973**, *241*, 20−22.

(23) Brown, K. R.; Walter, D. G.; Natan, M. J. *Chem. Mater.* **2000**, *12*, 306−313.

(24) Hoeppener, S.; Maoz, R.; Sagiv, J. *Nano Lett*. **2003**, *3*, 761−767.

(25) According to X-ray reflectivity data, the thickness of a complete, highly ordered NTS monolayer is ∼2.7 nm, with a characteristic roughness parameter (at the top monolayer surface) of ca. 0.2−0.4 nm.[13,19,20]

(26) Because of various possible artifacts of the SFM imaging, the SFM-measured heights of nanoobjects such as the present self-assembled organic bilayer features are not necessarily identical to their real heights. For example, complete and incomplete NTS top layers are expected to behave differently under the compressive forces exerted by the tip, less rigid incomplete overlayer features suffering larger deformations that translate into lower apparent heights. To minimize the role of artifactal effects originating in different imaging conditions, a comparative evaluation of the SFM-measured heights of different features should be done on a relative basis, from images taken with the same tip and under identical image recording conditions. Ideally, all compared features are located within the scan range of a single image. This condition is fulfilled in the case of the array of dots discussed here, which allows a valid comparison of the relative heights of 81 individual dot features, and thus a direct evaluation of the reproducibility of the patterning and subsequent overlayer assembly processes.

(27) For complete OTS/Si monolayers, the roughness of the OTS-coated surface is slightly lower than that of the uncoated silicon wafer substrate.

(28) Maoz, R.; Sagiv, J., unpublished results.

(29) Hoeppener, S.; Maoz, R.; Sagiv, J., to be submitted for publication.

NL049755K